Available online at www.sciencedirect.com
ScienceDirect
Journal of Organometallic Chemistry 691 (2006) 4660–4666
Journal of Organometallic Chemistry
www.elsevier.com/locate/jorganchem

Electrocatalytic reductive dimerization of the 2,2′-bipyridyl tungsten alkylidyne complex [W(≡$CC_6H_4NMe_2$-4)(NCMe)$(CO)_2$-{κ^2-2,2′-$(NC_5H_4)_2$}]$^+$

Elizabeth A. Duplessis, Paul A. Jelliss *, Charles C. Kirkpatrick, Shelley D. Minteer, Keith M. Wampler

Department of Chemistry, Saint Louis University, 3501 Laclede Avenue, St. Louis, MO 63103, USA

Received 16 June 2006; received in revised form 6 July 2006; accepted 13 July 2006
Available online 3 August 2006

Abstract

Potentiometric measurements have shown that the cationic 2,2′-bipyridyl tungsten alkylidyne complex [W(≡$CC_6H_4NMe_2$-4)(NCMe)$(CO)_2${κ^2-2,2′-$(NC_5H_4)_2$}][PF_6] (**2**) is electroactive in MeCN solution with a reduction ($E_{pc} \approx -1.0$ V vs. ferrocene) leading to complex dimerization, identified by a number of electrochemical markers. Multiple redox cycles have led to the partial deposition of the dimerized product on the electrode surface, which appears to electrocatalyze subsequent coupling cycles. Comparison with electrochemical measurements of related alkylidyne complexes, including the precursor complex [W(≡$CC_6H_4NMe_2$-4)$(O_2CCF_3)(CO)_2${κ^2-2,2′- $(NC_5H_4)_2$}] (**1**), has provided indirect evidence of intermolecular bond formation between κ^2-2,2′-bipyridyl ligands. The cationic complex **2** has additionally been the subject of GAMESS computational analysis, revealing calculated ν_{max}(CO) stretching absorptions in good agreement with measured parameters. This study has also permitted a molecular orbital analysis, which has indicated an energy-accessible LUMO almost entirely located on the 2,2′-bipyridyl ligand of complex **2**, the purported site for dimerization. It is believed that occupation of this orbital upon reduction of compound **2** leads to a short-lived metastable precursor to 2,2′-bipyridyl ring coupling. Furthermore, a very weak π-antibonding interaction of the metal–alkylidyne π-framework with the MeCN ligand in the occupied frontier molecular orbitals of complex **2** has been noted and compared with a surprisingly significant π interaction with the $CF_3CO_2^-$ carboxylate group in complex **1**.

Keywords: Tungsten; Alkylidyne; Dimerization

1. Introduction

The optoelectronic properties of Group 6 metal Fischer alkylidynes have been investigated to a limited extent with, for example, reports of photoluminescence in the TMEDA alkylidyne complex [W(≡CPh)Cl$(CO)_2${κ^2-$Me_2N(CH_2)_2$-NMe_2}] (TMEDA = *N*,*N*,*N*′,*N*′-tetramethylethylenediamine) and related cyclopentadienide derivatives [M(≡CAr)(CO){$P(OMe)_3$}(η^5-C_5H_5)] (M = W, Mo; Ar = Ph, C_6H_4Me-2, $C_{10}H_7$-2) [1,2]. The photophysical properties of other d^0–d^2 tungsten alkylidyne complexes have also been reviewed [3]. We have recently reported a substantially enhanced photoluminescent response in the complex [W(≡$CC_6H_4NMe_2$-4)$(O_2CCF_3)(CO)_2${κ^2-2,2′-$(NC_5H_4)_2$}] (**1**) and its cationic derivative [W(≡$CC_6H_4NMe_2$-4)(NCMe)$(CO)_2${κ^2-2,2′-$(NC_5H_4)_2$}][PF_6] (**2**) [4].

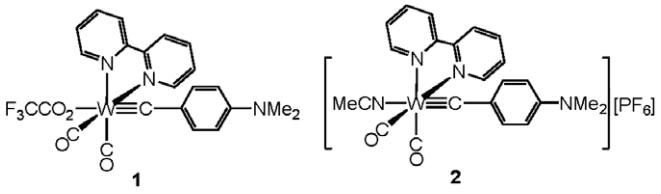

* Corresponding author. Tel.: +1 314 9772834; fax: +1 314 9772521.
E-mail address: jellissp@slu.edu (P.A. Jelliss).

0022-328X/$ - see front matter © 2006 Elsevier B.V. All rights reserved.
doi:10.1016/j.jorganchem.2006.07.029

Neutral complex **1** exhibits dual blue-yellow fluorescence ($\lambda_{em} = 450$, 580 nm) in CH_2Cl_2 solution at ambient temperatures, while **2** displays only blue emission ($\lambda_{em} = 450$ nm), attributed to a twisted intramolecular charge transfer (^{1}TICT) excited state.

2. Results

2.1. Electrochemistry

Despite this interesting photophysical behavior, CV (cyclic voltammetry) analysis of complex **1** would indicate little to get excited about, with an irreversible reduction at $E_{pc} \approx -1.8$ V in MeCN and THF, and no other redox processes observed within the solvent windows. However, CV analysis of the salt **2** combined with 1 mol equiv. of Fc (ferrocene) in MeCN revealed an unexpected apparently reversible reduction comprising an asymmetric cathodic wave with a peak at $E_{pc} = -1.09$ V vs. Fc (Fig. 1). This follows a sharp inflexion point characteristic of adsorption effects, despite the use of a glassy carbon working electrode, where such effects are normally minimized [5].

The return sweep oxidation peak at $E_{pa} = -0.95$ V yields $\Delta E_p = 146$ mV vs. 68 mV for the internal Fc standard at 0.1 V s^{-1}. This discrepancy is unlikely to be due to slow electron transfer kinetics, and more likely due to the oxidation of a completely new species. The peak ratio for the analyte cathodic process vs. the Fc anodic process, $i_{pc}/i_{pa,Fc} = 0.84$ suggests a 1-electron process for the reduction of complex **2** (vide infra). The peak current for the reverse oxidation, i_{pa}, however, is inflated ($i_{pa}/i_{pc} = 2.03$) and its asymmetric peakshape is indicative of electrode stripping as a consequence of adsorption upon reduction. Notwithstanding the asymmetric appearance of the cathodic wave, the reduction process is nevertheless diffusion controlled with a linear i_{pc} vs. $v^{1/2}$ plot (Fig. 2). This is not quite the case for the anodic process, which is clearly influenced by the adsorption/stripping, although deviation from linearity is slight over the scan rate range 0.05–0.90 V s^{-1}.

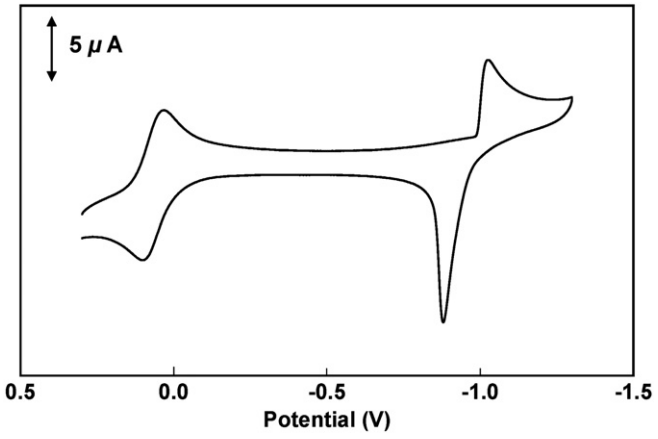

Fig. 1. CV of salt **2** + 1 mol equiv. Fc (MeCN, 500 μM, 0.10 V s^{-1}) vs. Ag/AgNO$_3$ (MeCN, 10 mM).

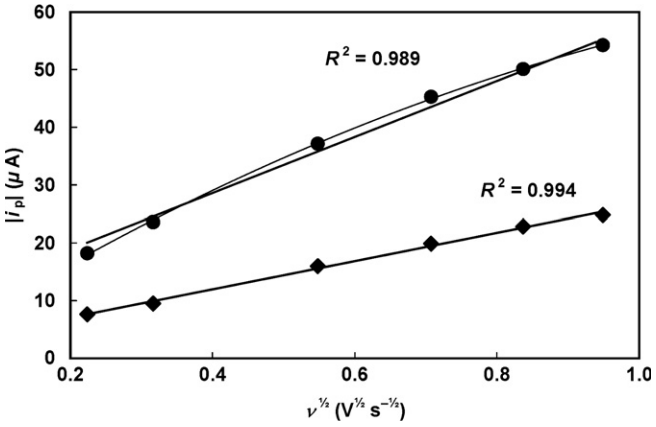

Fig. 2. Diffusion control $v^{1/2}$ vs. $|i_p|$ plots for the reduction of complex **2** (MeCN, 225 μM): (♦) cathodic scan; (●) anodic scan.

For a 10-fold increase in scan rate it was shown that $\Delta E_{pc} = -25$ mV. This is suggestive of a dimerization process involving the reduced species, being close to the theoretical value of −20 mV, and is supported by a linear plot of ln(scan rate), ln(v), vs. E_{pc} for a 1000 μM solution (Fig. 3a) with slope -9.99×10^{-3} V, near to that expected (-8.43×10^{-3} V) for a dimerization process [6]. A plot of ln(bulk molarity), ln(C), vs. E_{pc} (Fig. 3b) was also linear [6]. Unfortunately, it seems that if an $\vec{\mathbf{E}}_{rev}C_{2irrev}$ mechanism is operating, the dimerization step is so rapid that we are unable to observe the reoxidation of the monomer, even at scan rates up to 15 V s^{-1}. This makes assignment of an $E_{1/2}$ value tenuous at best and does not permit us to estimate the dimerization rate constant at this juncture.

A multiscan analysis (Fig. 4) was revealing. As expected with adsorption on the electrode, the anodic peak current increases with subsequent potential returns. Integrated charge calculations produced a q_{a10}/q_{c1} ratio of $\geqslant 4.8$, indicating the deposition of the equivalent of at least 4–5 monolayers on the electrode surface following 10 full sweeps. Interestingly, cathodic peak potentials became more positive by ca. +0.1 V toward the end of the 10 cycles, indicating electrocatalysis by the deposited material. Further evidence for electrocatalytic behavior may be extracted from the molarity-dependence plot in Fig. 3b in that the

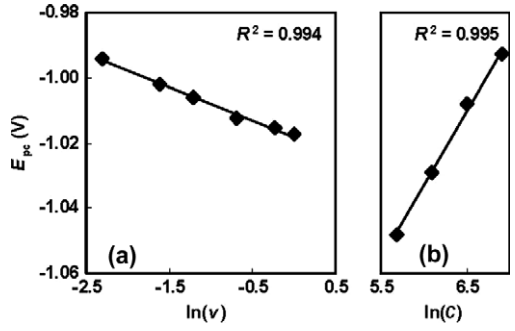

Fig. 3. Plot of cathodic peak potential, E_{pc} vs.: (a) ln(v) for scan rates, $v = 0.1$, 0.2, 0.3, 0.5, 0.8, 1.0 V s^{-1} for a 1000 μM MeCN solution of salt **2**; (b) ln(C) for [**2**] = 300, 440, 670, and 1000 μM ($v = 0.1$ V s^{-1}).

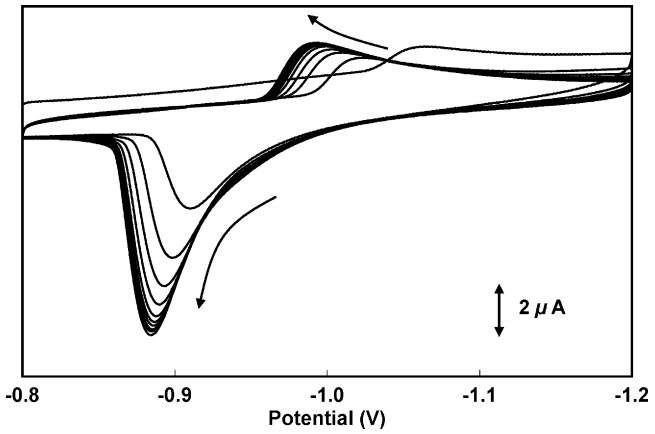

Fig. 4. CV (10 cycles) of salt **2** (MeCN, 500 μM, 0.05 V s^{-1}) vs. $Ag/AgNO_3$ (MeCN, 10 mM).

slope (+0.0457 V) is about 5 times the magnitude expected ($+8.43 \times 10^{-3}$ V).

Chronoamperometric analysis yielded the Cottrellian *i*–*t* transients just beyond the charging current observed in Fig. 5. A good linear fit [7] for the data points in the diffusion-limited field permits an accurate determination of the diffusion coefficient ($D = 2.7 \pm 0.1 \times 10^{-6}$ cm^2 s^{-1}) for an $n = 1$ reduction process with the cationic complex of **2**. Absolute values for diffusion coefficients should be treated with caution when adsorption effects are present. However, under the same conditions (following one reduction/adsorption/oxidation cycle of complex **2** at the working electrode) and using the same protocol, a diffusion coefficient for the ferrocene was estimated ($D_{Fc} = 4.5 \pm 0.2 \times 10^{-6}$ cm^2 s^{-1}). Neglecting any changes in concentration, this leads to a predicted peak current ratio of $i_{pc}/i_{pa,Fc} \approx 0.7$ [8], reasonably close to that observed (vide supra) and which supports the notion of a one-electron process. For the reduced product, the diffusion coefficient relating to the return oxidative step cannot be accurately determined because of interference from adsorption effects. However, it is evident from the markedly reduced linear regression slope of the plot that diffusion in this regime is likely to be slower than for the cationic starting complex, irrespective of the number of electrons involved in the anodic process (since slope $\sim nD^{1/2}$). Given that 1-electron reduction is expected to produce a neutral moiety, where less drag is expected to be exerted by the polar MeCN solvent and charged electrolyte molecules than on the starting cationic complex, one would expect an increase in the diffusion coefficient, if any change at all. Additionally if an $n = 2$ anodic process is operating as we suspect, there should indeed be a discernible increase in the slope for this plot. A decrease in slope (and therefore *D*) could therefore be a further indicator of the substantially greater molecular mass of the species being reoxidized.

It is noteworthy that CV analysis of the related complex $[W(\equiv CC_6H_4NMe_2\text{-}4)(NCMe)(CO)_2\{\kappa^2\text{-}Me_2N(CH_2)_2N\text{-}Me_2\}][PF_6]$ (**3**) [4], where an aliphatic TMEDA ligand replaces 2,2′-bipyridyl, showed no such reversible redox processes or any deposition, with an irreversible reduction at $E_{pc} = -1.70$ V in MeCN vs. Fc under similar conditions.

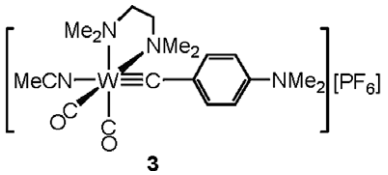

3

2.2. Microscopy

A visible thin film with a distinctly bluish hue is left on the glassy carbon working electrode following several scan cycles in the CV of compound **2**. It appears that the build-up does not exceed 4–5 monolayers, irrespective of the number of scan cycles beyond about 10, probably due to redissolution in the electrolyte solvent following oxidation. In fact, when freshly coated electrodes were dipped in neat MeCN, the deposit did ultimately dissolve and EPR analysis of these solutions yielded no evidence of a paramagnetic species. SEM analysis of the material deposited on gold foil working electrodes showed it to be a microporous deposit, with variable (1–10 μm) pore size (Fig. 6). A highly non-uniform deposition casts doubt upon electropolymerization as an outcome and supports the notion of an agglomerized molecular species, which is partially displaced from solution due to rapidly accumulating concentrations

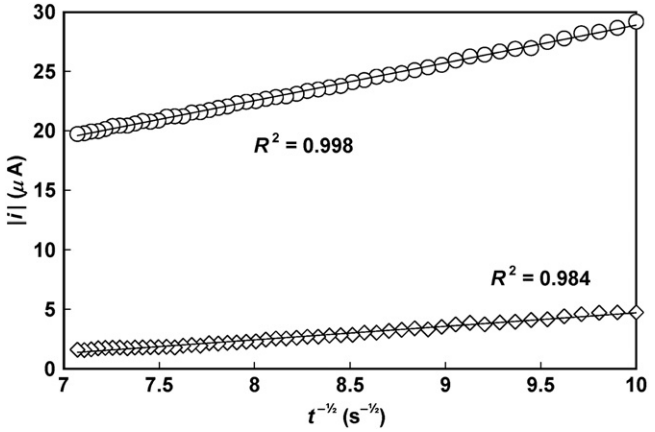

Fig. 5. Cottrell plots from chronoamperometry of salt **2** (MeCN, 500 μM, pulse width, $\tau = 20$ ms): (○) (−0.8 to −1.1 V); (◇) (−1.1 to −0.8 V). Data plotted for the 10–20 ms portion of each pulse.

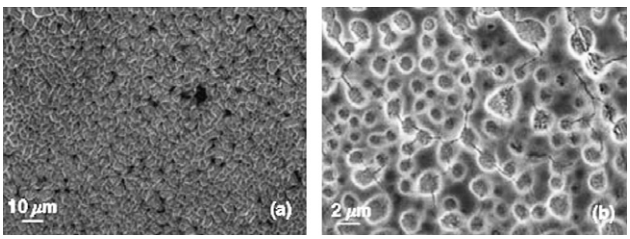

Fig. 6. SEM analysis of electrodeposited material from multiple CV cycles of compound **2** on a gold foil electrode surface at: (a) ×1800; (b) ×5500 magnification.

at the electrode, adhering to the electrode surface. XPS analysis (Table S1.1, Supplementary Data) of the deposit showed W content to be ⩽0.2 atom%; a value some 10 times greater might otherwise be expected for a pure W-containing compound. However, elevated P and F content was apparent (ca. 2% and 12%, respectively) indicating the presence of trapped $[NBu^n_4][PF_6]$ electrolyte in the deposit. This was verified by ^1H and $^{31}P\{^1H\}$ NMR analysis of a MeCN-d_3 solution of the residue. Indeed, the microporous structure of the deposit might well be attributed to the partial redissolution of the more soluble electrolyte before the electrode is removed from the solution.

2.3. Computational analysis

DFT Geometry energy minimizations were performed at the B3LYP level on compounds **1** and **2**. Electronic files containing atomic Cartesian coordinates for both computed structures are given in Supporting Data. The computational effort was reduced by constraining the molecules to having C_s symmetry In the absence of this constraint the geometry minimization did not converge, but iterated about a series of local energy minima resulting from rotation about the W–alkylidyne bond. Thus, all calculations were performed with the aryl ring *ipso–ortho* C–C bonds subtended at fixed torsion angles, $\tau_1 = -\tau_2 = 52.9°$ relative to the corresponding *syn* W–N(2,2′-bipyridyl) connectivities (Fig. 7). This is not unreasonable given the observed alkylidyne aryl orientation in the structurally characterized TMEDA–alkylidyne complex [W{≡CC_6H_4-4—C≡C—C_6H_4C(H)O-4}(Cl)$(CO)_2$\{κ^2-$Me_2N(CH_2)_2NMe_2$\}], where the torsion angles, $\tau_1 = 53.4°$, $\tau_2 = -52.0°$ relative to the corresponding *syn* W–N(TMEDA) connectivities as measured from data in the available CIF file [9]. That said, the same report describes the X-ray structure of the complex [W(≡CC_6H_4I-4)(Cl)$(CO)_2$\{κ^2-$Me_2N(CH_2)_2NMe_2$\}], where $\tau_1 = -4.5°$, $\tau_2 = -108.6°$, i.e. the aryl ring is almost aligned with the W–N_1 bond and is approximately half way between perfect C_s structures. This would seem to indicate the propensity of the alkylidyne aryl system to adopt more than one rotational conformation about the W≡C bond with similar gross energy minima.

There are no previously characterized X-ray structures of 2,2′-bipyridyl-alkylidyne complexes with which to make the same comparative evaluation. However, in a further comparison of compounds **1** and **2** with existing W–alkylidyne complexes, the W≡C bond lengths were computed at 1.88 Å (**1**) and 1.89 Å (**2**), slightly longer but on a par with those found in either of these TMEDA complexes (1.807(8) Å for [W(≡CC_6H_4I-4)(Cl)$(CO)_2$\{κ^2-$Me_2N(CH_2)_2NMe_2$\}] and 1.800(7) Å for [W{≡CC_6H_4-4—C≡C—C_6H_4C(H)O-4}(Cl)$(CO)_2$\{κ^2-$Me_2N(CH_2)_2NMe_2$\}]). The increased W≡C bond length for compounds **1** and **2** can simply be attributed to the aryl NMe_2 donor group, resulting in a hyperconjugative effect that also manifests itself in slightly shorter calculated alkylidyne-C–aryl-*ipso*-C bond lengths for **1** (1.42 Å) and **2** (1.40 Å) than for [W(≡CC_6H_4I-4)(Cl)$(CO)_2$\{κ^2-$Me_2N(CH_2)_2NMe_2$\}] (1.46(1) Å) and [W{≡CC_6H_4-4—C≡C—C_6H_4C(H)O-4}(Cl)$(CO)_2$\{κ^2-$Me_2N(CH_2)_2NMe_2$\}] (1.454(9) Å) as one might expect.

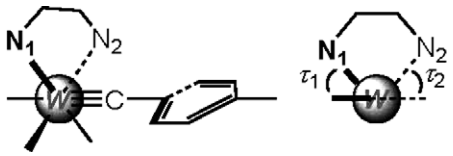

Fig. 7. Torsion angles, τ, between the alkylidyne aryl *ipso–ortho* C–C bonds and the *syn* W–N bonds of the bidentate *N*-donor ligand (pairs of bonds shown as bold (—) and dashed (---) connectivities).

MO (molecular orbital) analysis of the geometry-minimized complex cation **2** yielded MO energies (Table S2.1, Supplementary Data) as well as the corresponding MO fragmental electron density distribution for the key components of the complexes (Table S2.2, Supplementary Data). In particular this data revealed a 2,2′-bipyridyl-centered (91%) LUMO (131) (Fig. 8). There is a HOMO–LUMO energy gap of 2.37 eV and the lower-lying occupied MOs 130 and 128 are clearly orthogonal metal–alkylidyne-aryl π-bonding in nature with MO 130 destabilized some 1.16 eV by interaction with the aryl NMe_2 lone pair. In this narrow energy group of occupied orbitals, HOMO − 1 (129) involves essentially metal–carbonyl $W(CO)_2$ d_π–π^* interactions (69% W, 24% CO).

The MeCN ligand in compound **1** is antibonding with respect to the W metal center in HOMO − 2 (128) and HOMO (130). The very small contribution (<2%) of the MeCN ligand to the total density of these MO's, however, minimizes the impact of this destabilizing electronic interaction. When the π-bonding MeCN ligand was replaced by NMe_3 in compound **1**, there was little resulting impact on the overall frontier molecular orbital energy scheme, as is apparent from the relatively unchanged energy levels in Fig. 8 and their fragment composition, thus supporting the minimal contribution of π^*-antibonding between MeCN and W. A similar computation on the parent neutral alkylidyne complex **1** revealed almost identical MOs, but displaced 0.07–0.17 eV higher in energy, although we note a greater contribution from the alkylidyne moiety to HOMO − 1 (146) of complex **1** (12% vs. 1% in MO 129 in complex **2**). Even though the overall complex charge (or lack thereof) must clearly impact the MO energy levels, unlike the MeCN ligand of complex **2** (2% contribution to both MO 128 and 130), W–ligand π-bonding contributions of the carboxylate group to HOMO (147) and HOMO − 2 (145) are no longer insignificant (6% and 16%, respectively), especially for the latter. Such metal–ligand d_π–π_{CO2} orbital overlap may indeed be facilitated by the orientation of the carboxylate C═O group toward the charge deficient 2,2′-bipyridyl ligand bridgehead carbon atoms. This is not surprising given the charge distribution based on atomic Mulliken charge calculations (Table 1). Although such a model makes perfect sense from an electrostatic perspec-

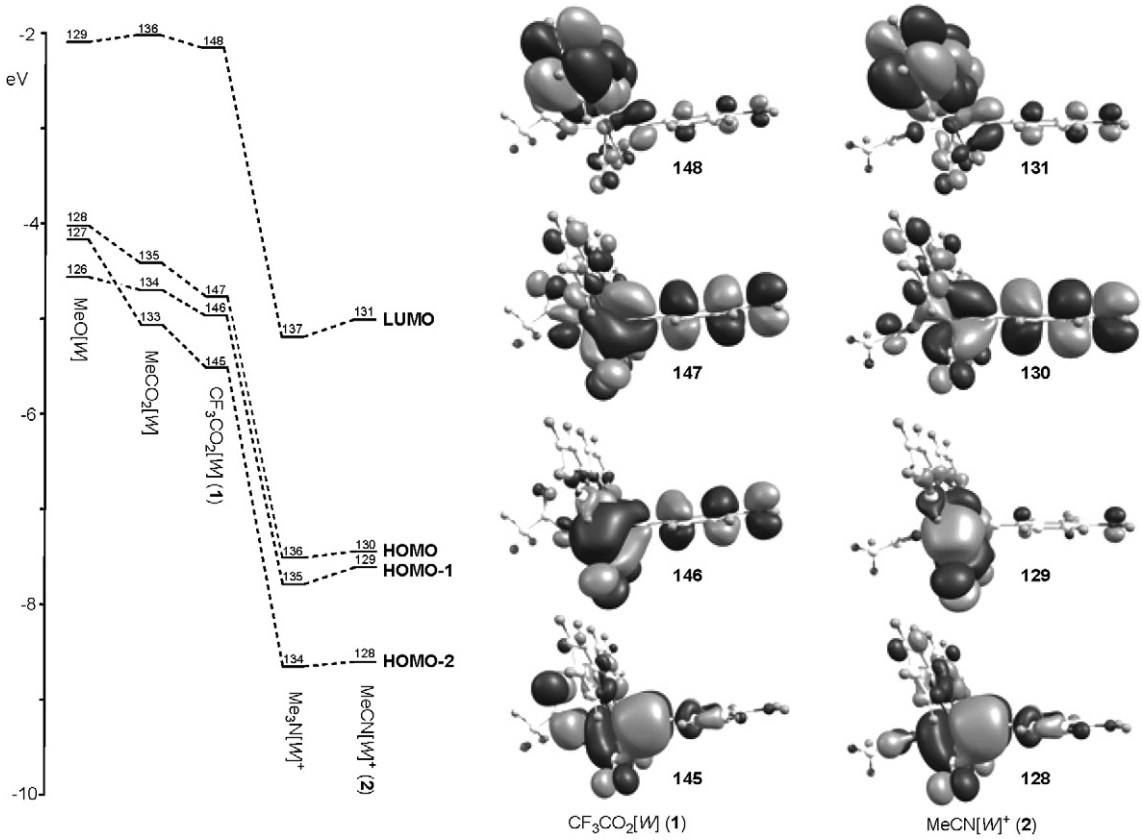

Fig. 8. Calculated LUMO, HOMO, HOMO − 1, and HOMO − 2 energies for geometry-minimized tungsten alkylidyne complexes $L[W]^{n+}$, where $L[W]^{n+} = [W(\equiv CC_6H_4NMe_2\text{-}4)(L)(CO)_2\{\kappa^2\text{-}2,2'\text{-}(NC_5H_4)_2\}]^{n+}$ ($n = 1$, L = NCMe, NMe_3; $n = 0$, L = O_2CCF_3, O_2CMe, OMe). These MOs are also rendered for the complexes **1** and **2**. Precise orbital energies are given in Table S2.1 in Supplementary Data.

Table 1
Mulliken charge and bond stretching frequency calculations for complexes **1** and **2**[a]

Mulliken charges

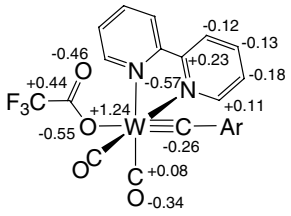

1

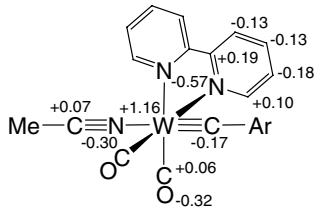

2

IR stretching frequencies	Observed[b]	Calculated	Observed[b]	Calculated
ν_{max}(CO) (cm^{-1})	1973, 1888	1968[c], 1916[d]	1981, 1900	1990[c], 1936[d]
ν_{max}(CO_2) (cm^{-1})	1689	1678[d]	–	–
ν_{max}(CN) (cm^{-1})	–	–	2254	2302

[a] B3LYP calculations based on Huzinaga's 21 split valence set. Constrained C_s symmetry necessitates showing charges on only one CO and one of the 2,2′-bipyridyl rings.
[b] Ref. [4].
[c] Symmetric stretch.
[d] Antisymmetric stretch.

tive, we have been unable to procure tractable single crystals of complex **1** to verify this configurational arrangement. However, the impact of the π-donor ability of the ligands on the complex HOMOs can be seen by substituting the $CF_3CO_2^-$ ligand with the increasingly powerful π-donor ligands $MeCO_2^-$ and MeO^-, respectively (Fig. 8). The HOMO energies are clearly displaced upwards with increasing W–ligand π* interaction, while the variation in LUMO is minimal. This again serves to emphasize the independence of the 2,2′-bipyridyl-based LUMO from the

cis-ligand which is itself *trans* to the alkylidyne carbon atom.

Given the stabilization of the LUMO in complex **2** relative to that of complex **1** and the observation that the ν_{max}(CO) peaks from the IR spectra for complexes **1** (1973, 1888 cm^{-1}) and **2** (1981, 1900 cm^{-1}) (Table 1) are not all that different, in addition to the similar ^{13}C NMR chemical shifts of the alkylidyne carbons [δ 281.3 (**1**) and 282.1 (**2**)] [4], one might conclude that the level of electron density on the W≡C core is invariant between the two complexes despite their charge difference. The 2,2′-bipyridyl ligand therefore bears much of the brunt of the electronic charge depreciation upon forming **2** from **1**. The initially reduced paramagnetic complex $\mathbf{2}_{red}$ therefore might better be described as a metastable W(IV) d^2/bipy(−1) species rather than a formally metal-reduced W(III) d^3/bipy(0) moiety. Although a similar scenario may be envisaged with the reduction of complex **1**, rapid decomposition of this reduced species $\mathbf{1}_{red}$ must be occurring at the much lower potential, thus not affording an opportunity to couple in a similar manner.

3. Discussion

A likely scenario for post-reductive dimerization of complex $\mathbf{2}_{red}$ might seem to be the coupling of the acetonitrile ligands resulting in either bridging *anti*-butane-2,3-diiminato(2–)-*N*:*N*′ or (*E*)-butene-2,3-diimido(4–)-*N*:*N*′ ligands, given several reports of this phenomenon [10]. However, the above experimental observations and DFT calculations point toward intermolecular 2,2′-bipyridyl C–C reductive coupling. The absence of similar electrochemical behavior with compound **3**, in particular, diverts attention from the coordinated MeCN as the site for coupling as well as the alkylidyne ligand itself. Coupling should therefore occur most logically at the C^4-position, *para* to one of the coordinating nitrogens, generating two amido nitrogen lone pairs in a 4′,4″-dihydro-2,2′,4′,4″,2″,2‴-quarterpyridinyl dianion ligand assembly.

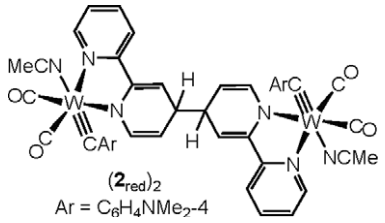

Similar C–C reductive coupling of coordinated κ^2-1,10-phenanthroline has been reported for the silicon-bound system $[Ru(PMe_3)_2(\eta^5\text{-}C_5Me_5)\{Si(SC_6H_4Me\text{-}4)(\kappa^2\text{-}1,10\text{-}N_2C_{12}H_8)\}][CF_3SO_3]$ [11]. Another possibility for the formation of $(\mathbf{2}_{red})_2$ would involve coupling at the *ortho*-C^6 position, but this would be sterically much less accessible being closer to the metal, and is therefore kinetically less attractive. With $E_{pc} = -0.95$ V (vide supra), dissociation of 2,2′-bipyridyl ($E_{1/2} = -2.60$ V in DMF [12]) prior to reductive coupling is not an option. The fate of dimer $(\mathbf{2}_{red})_2$ beyond this point remains under investigation. While CV measurements suggest a 2-electron oxidative process may be occurring, there is no evidence as to whether this is metal- or ligand-centered. Ligand dissociation following the initial anodic scan and prior to adsorption on the electrode surface, for instance, cannot be ruled out and indeed, the low W% observed in the XPS analysis may also be a consequence of this.

Intermolecular reductive coupling of coordinated κ^2-2,2′-bipyridyl ligands has not been previously reported, but oxidative coupling has been observed both chemically and electrochemically following addition of 2,2′-bipyridyl to the complex $[Cr\{\kappa^2\text{-}(CH_2)_2SiMe_2\}(OC_4H_8)(\eta^5\text{-}C_5Me_5)]$ [13]. It should be mentioned, however, that the dimerization in this example occurs with the resulting adduct $[Cr(\kappa^3\text{-}2,2'\text{-}NC_5H_3\{2\text{-}CH_2Si(Me)_2CH_2\}NC_5H_4)(\eta^5\text{-}C_5Me_5)]$, which does not contain a pristine κ^2-2,2′-bipyridyl ligand, but one that has been modified by intramolecular transfer of one arm of the $(CH_2)_2SiMe_2$ ligand to the bridgehead carbon 2-C atom of one of the 2,2′-bipyridyl rings. With this in mind it is entirely possible that some irreversible intramolecular ligand transformation of the coupled bipyridyl ligands involving migration of the ene-amido-type nitrogen atom to the alkylidyne carbon, MeCN or even a CO ligand may also be occurring concomitant with or subsequent to the formation of $(\mathbf{2}_{red})_2$.

4. Conclusion

The chemistry described herein provides strong electrochemical evidence of dimerization upon potentiometric cycling of complex **2** at ca. −1.0 V vs. Fc. Comparison of experimental and computational results with the irreversible reductions of complexes **1** and **3** ($E_{pc} \approx -1.7$ V) strongly suggests (but does not prove) that the 2,2′-bipyridyl ligand is the location of the electrocoupling. Efforts to identify and characterize the final product, which undergoes partial deposition on the working electrode surface, are still in progress.

5. Experimental section

5.1. Electrochemistry

CV experiments were performed on complexes **1**–**3** (synthesized according to experimental methods given in Ref. [4]) with a CH Instruments electrochemical analyzer. All potentials were measured relative to an $Ag/AgNO_3$ (MeCN, 10 mM) reference electrode at 20 °C and quoted relative to an internal standard comprising the ferrocene/ferrocenium couple. All solutions were studied in a three-electrode cell under Ar in distilled, deoxygenated solvents and contained 0.1 M $[NBu^n_4][PF_6]$ as supporting electrolyte in MeCN. Measurements were made on a glassy carbon

disc working electrode with a surface area of 7.07 mm^2, which was polished, rinsed, and dried between measurements. The counter electrode was Pt wire and pre-cleaned by soaking in conc. HNO_3, rinsed and flame-dried. Chronoamperometry experiments were also run with the same electrodes, with potential limits determined from the CV experiment.

5.2. Microscopy

Scanning electron microscopy (SEM) was carried out with a JEOL JSM 5800 instrument. Substrate gold foil electrodes (ca. 1 cm^2) were coated in the electrochemical cell previously described by ca. 20 CV cycles. Substrates for X-ray photoelectron spectroscopy (XPS) were similarly electrocoated graphite disc electrodes and analysed by Evans Analytical Group, Round Rock, TX, USA, using a Physical Electronics 5500 ESCA/XPS instrument. Results are included as Supplementary Data.

5.3. Computational analysis

DFT geometry optimizations, molecular orbital and vibrational frequency calculations were performed with GAMESS-USA [14], using B3LYP model chemistry and Huzinaga's 21 split valence set [15]. Optimizations were constrained to having only C_s molecular symmetry. Starting geometries were based on bond distances and angles observed in compounds containing similar functional groups. The atomic Cartesian coordinates for compounds **1** and **2**, as well as a complete listing of energies and composition of LUMO, HOMO, HOMO − 1, and HOMO − 2 molecular orbitals, are available as Supplementary Data.

Acknowledgements

Financial support from the ACS Petroleum Research Fund and from the Saint Louis University Beaumont Faculty Development Fund.

Appendix A. Supplementary data

Supplementary data associated with this article can be found, in the online version, at doi:10.1016/j.jorganchem.2006.07.029.

References

[1] A.B. Bocarsly, R.E. Cameron, H.D. Rubin, G.A. McDermott, C.R. Wolff, A. Mayr, Inorg. Chem. 24 (1985) 3976.
[2] T.K. Schoch, A.D. Main, R.D. Burton, L.A. Lucia, E.A. Robinson, K.S. Schanze, L. McElwee-White, Inorg. Chem. 35 (1996) 7769.
[3] R.E. Da Re, M.D. Hopkins, Coord. Chem. Rev. 249 (2005) 1396.
[4] P.A. Jelliss, K.M. Wampler, A. Siemiarczuk, Organometallics 24 (2005) 707.
[5] A.J. Bard, L.R. Faulkner, Electrochemical Methods, Wiley, New York, 1980;
D. Astruc, Electron Transfer and Radical Processes in Transition-metal Chemistry, VCH, New York, 1995.
[6] Taken from the equation for the dimerization rate constant, k_{dim}, where $E_p = E_{1/2} - 0.047 + (8.43 \times 10^{-3})\ln k_{dim} + (8.43 \times 10^{-3})\ln(C/v)$, for a solution of molarity, C (μM), and scan rate, v (V s^{-1}). C.P. Andrieux, L. Nadjo, J.M. Saveant, J. Electroanal. Chem. 42 (1973) 223;
R.J. Forster, Phys. Chem. Chem. Phys. 1 (1999) 1543.
[7] Diffusion coefficient, D, calculated using the chromoamperometric i–t transients according to the Cottrell equation: $it^{1/2} = nFAC(D/\pi)^{1/2}$, where A is the electrode area (cm^2) and C is the bulk concentration (mol cm^{-3}). R.N. Adams, Electrochemistry at Solid Electrodes, Marcel Dekker, New York, 1969.
[8] Estimated peak current ratio for an irreversible versus a reversible electrochemical process calculated from the equation $i_{pc}/i_{pa,Fc} = (n/n_{Fc})(\alpha D/D_{Fc})^{1/2}$ ($\alpha = 0.5$) taken from Ref. [5].
[9] M.P.Y. Yu, K.-K. Cheung, A. Mayr, J. Chem. Soc., Dalton Trans. (1998) 2373.
[10] Y.-C. Tsai, F.H. Stephens, K. Meyer, A. Mendiratta, M.D. Gheorghiu, C.C. Cummins, Organometallics 22 (2003) 2902;
C.G. Young, C.C. Philipp, P.S. White, J.L. Templeton, Inorg. Chem. 34 (1995) 6412;
R. Duchateau, A.J. Williams, S. Gambarotta, M.Y. Chiang, Inorg. Chem. 30 (1991) 4863;
E.J.M. De Boer, J.H. Teuben, J. Organomet. Chem. 153 (1978) 53;
F.A. Cotton, W.T. Hall, Inorg. Chem. 17 (1978) 3525;
P.A. Finn, M.S. King, P.A. Kilty, R.E. McCarley, J. Am. Chem. Soc. 97 (1975) 220.
[11] S.D. Grumbine, R.K. Chadha, T.D. Tilley, J. Am. Chem. Soc. 114 (1992) 1518.
[12] E.J.L. McInnes, R.D. Farley, C.C. Rowlands, A.J. Welch, L. Rovatti, L.J. Yellowlees, J. Chem. Soc., Dalton Trans. (1999) 4203.
[13] S. Leelasubcharoen, K.-C. Lam, T.E. Concolino, A.L. Rheingold, K.H. Theopold, Organometallics 20 (2001) 182;
S. Leelasubcharoen, M.W. Lehmann, K.H. Theopold, D.H. Evans, J. Electrochem. Soc. 148 (2001) E118.
[14] M.W. Schmidt, K.K. Baldridge, J.A. Boatz, S.T. Elbert, M.S. Gordon, J.J. Jensen, S. Koseki, N. Matsunaga, K.A. Nguyen, S. Su, T.L. Windus, M. Dupuis, J.A. Montgomery, J. Comput. Chem. 14 (1993) 1347.
[15] S. Huzinaga, J. Andzelm, M. Klobukowski, E. Radzio-Andzelm, Y. Sakai, H. Tatewaki, GAUSSIAN Basis Sets for Molecular Calculations, Elsevier, Amsterdam, 1984.